

## THE SCATTERING OF X-RAYS BY INTERSTELLAR DUST ON THE MICROARCSECOND SCALE

DAVID L. WINDT

Bell Labs, Lucent Technologies, Room 1D-456, 600 Mountain Avenue, Murray Hill, NJ 07974; windt@bell-labs.com

WEBSTER CASH

Center for Astrophysics and Space Astronomy, University of Colorado, Campus Box 389, Boulder, CO 80309; wcash@casa.colorado.edu

AND

STEVEN M. KAHN

Columbia Astrophysics Laboratory, Columbia University, New York, NY 10027; skahn@astro.columbia.edu

Received 1999 February 5; accepted 1999 August 17

### ABSTRACT

We have calculated on a small angular scale the distribution of X-rays (e.g., as originating from a point source) scattered by interstellar dust. In addition to the well-known, large-diameter (i.e., hundreds of arcseconds) X-ray halo due to dust distributed along the line of sight to the source, we show that material clumped very close to the source gives rise to a bright, small-diameter (subarcsecond) X-ray halo. The diameter of this inner “microhalo” decreases, and the relative surface brightness increases, as the relative concentration of dust very near the source increases. For example, we expect that the 1 keV X-ray microhalo surrounding a point source in M87 would have a diameter of order 1 microarcsecond ( $\mu\text{as}$ ) and a surface brightness relative to the point source flux of order  $10^{-29} \mu\text{as}^{-2} \text{cm}^2 (\text{H atom})^{-1}$ , while the large-diameter halo due to scattering from dust within our own Galaxy would have a diameter of order  $100''$  and a relative surface brightness more than 12 orders of magnitude lower than the microhalo surface brightness. We discuss the consequences of our results with regard to future high-resolution X-ray imaging observations, and also with regard to the possibility of using detailed measurements of the X-ray halo profile to determine the spatial distribution of dust along the line of sight and close to the source.

*Subject headings:* dust, extinction — radiative transfer — scattering — X-rays: ISM

### 1. INTRODUCTION

X-ray halos due to scattering by interstellar dust grains have been observed for a variety of Galactic and extragalactic sources (Rolf 1983; Catura 1983; Bode et al. 1985; Mauche & Gorenstein 1986; Mauche & Gorenstein 1989; Gallagher, Cash, & Green 1995; Predehl et al. 1991; Mathis et al. 1995; Woo et al. 1994; Predehl & Schmitt 1995). In all cases reported thus far, halos were detected at an angular distance from the source of order  $1'$  or greater, consistent with the performance limitations of the instruments used to make the observations. However, future X-ray missions such as *Chandra* (*CXO*) will have greater sensitivity and subarcsecond angular resolution. On a longer timescale, space-based X-ray interferometry holds the promise of microarcsecond ( $\mu\text{as}$ ) angular resolution, or better, for observations of distant cosmic sources. At the  $\mu\text{as}$  level, a number of very exciting observational programs may become feasible, including imaging the event horizons of nearby extragalactic supermassive black holes (i.e., active galactic nuclei [AGNs]). However, such ultra-high-resolution observations might be compromised by blurring associated with dust scattering. In this paper we thus consider the scattering of X-rays by interstellar dust on the  $\mu\text{as}$  scale: we have made numerical simulations of the angular distribution of scattered X-rays for a variety of cases, using physically reasonable models for grain-size distributions. In § 2 we briefly review the theoretical basis on which our numerical simulations are based. In § 3 we present the results of these simulations, and in § 4 we discuss the impact these results may have on observations made with future high-resolution X-ray telescopes.

### 2. THEORY

We compute the scattering of X-rays by interstellar dust grains using the Rayleigh-Gans (RG) approximation for the differential scattering cross section ( $d\sigma/d\Omega$ ). As discussed in detail by Smith & Dwek (1998, hereafter SD), the RG approximation is valid when both (a) reflection from the surface of the dust grain is negligible, and (b) the phase of the incident wave is not shifted inside the dust grain. Condition *a* is met when  $|n-1| \ll 1$ , where  $n$  is the complex index of refraction of the dust, and certainly applies to the case of normal graphite or silicate grains at X-ray energies greater than 1 keV. As shown by SD, condition *b* is met when

$$\frac{a_{\mu\text{m}}}{E_{\text{keV}}} \left( \frac{\rho}{3 \text{ g cm}^{-3}} \right) \ll 0.316, \quad (1)$$

where  $a_{\mu\text{m}}$  is the dust-grain radius in microns,  $E_{\text{keV}}$  is the photon energy in keV, and  $\rho$  is the grain density in  $\text{g cm}^{-3}$ ; the “rule of thumb” is thus that the RG approximation is valid only if the photon energy in keV is significantly larger than the dust-grain radius in  $\mu\text{m}$ , for grains of normal composition (i.e., graphite, silicates, etc.) We thus consider below scattering by X-rays having energies above 1 keV, by graphite and/or silicate dust grains having radii less than  $\sim 0.25 \mu\text{m}$ .

The differential cross section for scattering at an angle  $\theta_{\text{sca}}$  by a single (spherical) dust grain of radius  $a$  is given in the RG approximation by Mauche & Gorenstein (1986,

hereafter MG) as

$$\frac{d\sigma_{\text{sca}}(\theta_{\text{sca}})}{d\Omega} = c_1 \left( \frac{2Z}{M} \right)^2 \left( \frac{\rho}{3 \text{ g cm}^{-3}} \right)^2 a(\mu\text{m})^6 \times \left[ \frac{F(E)}{Z} \right]^2 \Phi^2(\theta_{\text{sca}}), \quad (2)$$

where  $c_1 = 1.1 \text{ cm}^2/\text{sr} = 2.6 \times 10^{-23} \text{ cm}^2 \mu\text{as}^{-2}$ ,  $Z$  is the mean atomic charge,  $M$  is the mean molecular weight (amu),  $\rho$  is the grain mass density,  $F(E) = |f_1 + if_2|$  is the grain atomic scattering factor at energy  $E$ , and  $\Phi(\theta_{\text{sca}})$  is the “form factor,” given by

$$\Phi(\theta_{\text{sca}}) = 3(\sin u - u \cos u)/u^3, \quad (3)$$

where

$$u \equiv 2\pi a \theta_{\text{sca}} E/hc = 1.474 a_{\mu\text{m}} \theta_{\text{arcmin}} E_{\text{keV}}/(1-x) \quad (4)$$

and  $x$  is the fractional distance to the source, with  $0 < x < 1$ . The observation angle is related to the scattering angle by  $\theta = (1-x)\theta_{\text{sca}}$ .

Mathis & Lee (1991, hereafter ML) considered the contribution to the X-ray halo surface brightness from single as well as multiple scattering events. In essence they find that multiple scattering events are generally important, resulting in an increase of the brightness of the halo at large angles (roughly equivalent to the effect of having a large fraction of small-diameter grains); at small scattering angles, the halo brightness is dominated by the single-scattering events. However, the brightest X-ray halos occur when the optical depth to scattering is low; when the optical depth for scattering is high enough that multiple scattering is important, absorption along the line of sight greatly reduces both the source and halo intensity (SD; Predehl & Klose 1996). We have thus considered only single-scattering events, in which case the halo surface brightness at an observation angle  $\theta$  is given by

$$I_{\text{sca}}(\theta) = F_x N_{\text{H}} \int dE S(E) \int da n(a) \int df(x) (1-x)^{-2} \times \left[ \frac{d\sigma_{\text{sca}}(a, E, \theta, x)}{d\Omega} \right], \quad (5)$$

where  $F_x$  is the observed source flux ( $\text{photons cm}^{-2} \text{ s}^{-1}$ ),  $N_{\text{H}}$  is the column density of hydrogen (in all forms),  $S(E)$  is the (normalized) photon energy of the source,  $n(a)da$  is the number of grains (per H atom) with radii between  $a$  and  $a + da$ , and  $f(x)$  is the (normalized) distribution of hydrogen along the line of sight to the source.

### 3. RESULTS

Numerically integrating equation (5), we have computed the relative X-ray halo surface brightness,  $I_{\text{sca}}(\theta)/F_x/(N_{\text{H}})$ , for a variety of cases. We first consider the case of single-sized dust grains distributed uniformly along the line of sight from  $x = 0$  to  $x = x_{\text{max}}$ . We assume a mixture of graphite ( $\rho = 2.3 \text{ g cm}^{-3}$ ) and olivine ( $\text{Fe, Mg}_2\text{SiO}_4$ ,  $\rho = 3.3 \text{ g cm}^{-3}$ ) grains, having radii  $a = 0.2 \mu\text{m}$ . The total mass of dust grains (relative to the H column) along the line of sight has been set equal to the value obtained using the Mathis, Rumpl, & Nordsieck (1977, hereafter MRN) grain model described below, and we have used the atomic scattering factors from Henke et al. (1993).

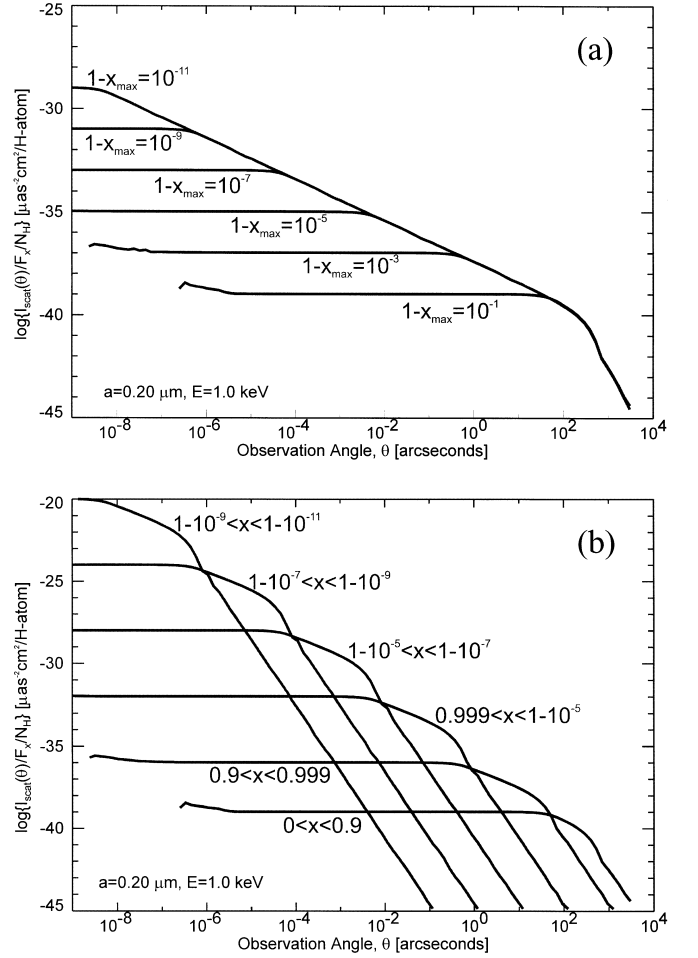


FIG. 1.—Relative X-ray halo surface brightness,  $\log [I_{\text{sca}}(\theta)/F_x/(N_{\text{H}})]$  as a function of observation angle  $\theta$  at a photon energy  $E = 1 \text{ keV}$ , assuming single-sized dust grains ( $a = 0.2 \mu\text{m}$ ) (a) distributed uniformly along the line of sight from  $x = 0$  to  $x = x_{\text{max}}$ , and (b) distributed uniformly from  $x = x_{\text{min}}$  to  $x = x_{\text{max}}$ , for various values of  $x_{\text{min}}$  and  $x_{\text{max}}$  as indicated.

Shown in Figure 1a is a log-log plot of the resultant X-ray halo surface brightness at an energy  $E = 1 \text{ keV}$ , for a range of  $x_{\text{max}}$  values such that  $(1 - x_{\text{max}})$  ranges from  $10^{-1}$  to  $10^{-11}$ . There are two “shoulders” in each of the curves shown in Figure 1a: for a given value of  $x_{\text{max}}$ , the halo intensity is roughly constant for  $\theta < \theta_{\text{max}}$ , i.e., the position of the first, inner shoulder [where  $\log(\theta_{\text{max}})$  scales with  $(1 - x_{\text{max}})$ ], and then decreases monotonically out to  $\theta \sim 200''$  (i.e., the second, outer shoulder), at which point the halo intensity then decreases much more rapidly with increasing  $\theta$ . The large-diameter outer shoulder is typical of X-ray halos observed, for example, by MG.

In Figure 1b, we show a similar result, except now the concentration of dust is uniform between  $x_{\text{min}}$  and  $x_{\text{max}}$ , and is zero everywhere else. In this case there is only a single, broad shoulder in the scattered X-ray surface brightness profile, and because the same amount of dust is now contained in a relatively thin layer between  $x_{\text{min}}$  and  $x_{\text{max}}$  the halo surface brightness values (i.e., per  $N_{\text{H}}$ ) are much larger as compared to the previous case (Fig. 1a). As the relative concentration of dust very near the source increases, the diameter of the “microhalo” decreases, and the relative surface brightness increases as a result of the larger incident flux brightness, which scales as  $(1-x)^{-2}$ , where  $(1-x)$  is the distance from the source to the scattering layer of dust.

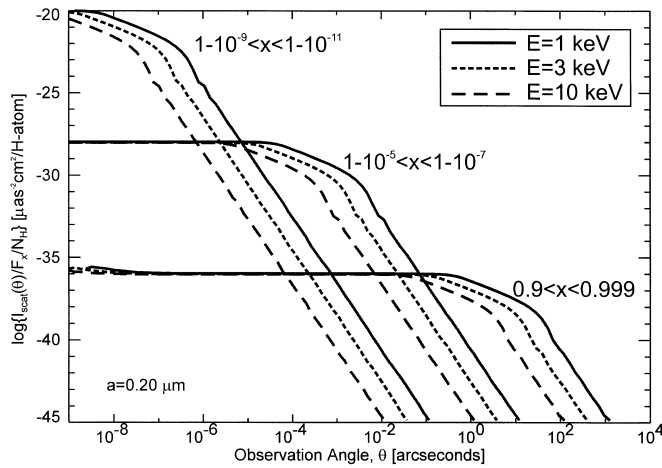


FIG. 2.—Similar to Fig. 1b, but for three different photon energies, as indicated.

In the case where the dust is confined between  $10^{-9} < 1 - x < 10^{-11}$ , for example, at 1 keV a hydrogen column density of  $10^{22} \text{ cm}^{-2}$  would produce a  $\sim 1 \mu\text{as}$  X-ray halo having a surface brightness equal to  $\sim 10^{-4}$  times the point-source flux.

Next we consider the dependence of the scattered X-ray surface brightness profile on photon energy and grain-size distribution. Shown in Figure 2 are the X-ray halo profiles for three X-ray energies—1, 3, and 10 keV—again using a single dust-grain size ( $0.2 \mu\text{m}$ ) distributed uniformly between  $x_{\min}$  and  $x_{\max}$ . As in the case of the large-diameter X-ray halos considered by ML, we find that both the halo diameter and the intensity of scattered light at large angles (i.e., outside the shoulder) decrease with increasing photon energy.

In Figure 3 we keep the energy fixed at 1 keV, and vary the grain-size distribution: curves are shown for two cases using single grain sizes— $0.02 \mu\text{m}$  and  $0.2 \mu\text{m}$ —and also for the MRN grain model. The MRN model assumes a power-law distribution for graphite and silicate grains, with 100% of the cosmic abundance of silicon in grains of olivine ( $\text{Fe, Mg}_2\text{SiO}_4$ ), and with 60% of the cosmic abundance of

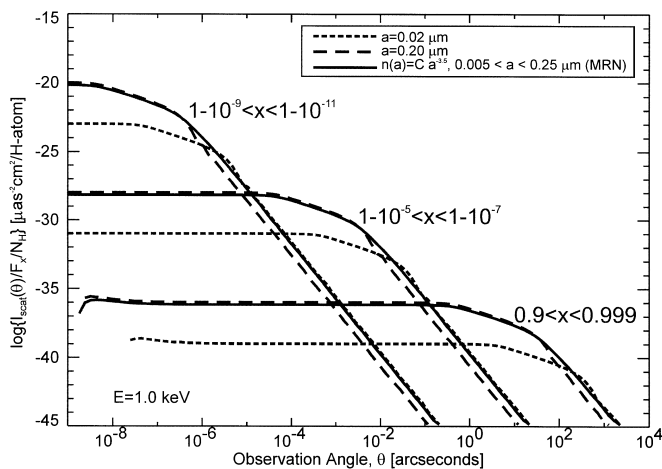


FIG. 3.—Relative X-ray halo surface brightness as a function of observation angle  $\theta$  at a photon energy  $E = 1 \text{ keV}$ , for single-size dust grains of radius  $a = 0.02 \mu\text{m}$  and  $a = 0.2 \mu\text{m}$ , and for the MRN grain model described in the text.

carbon in graphite grains:

$$n(a)da = Ca^{-3.5}da, \quad (6)$$

where for graphite  $C = 5.75 \times 10^{-16} (\text{H atom})^{-1} \mu\text{m}^{2.5}$ ,  $0.005 \mu\text{m} < a < 0.25 \mu\text{m}$  while for olivine  $C = 6.17 \times 10^{-16} (\text{H atom})^{-1} \mu\text{m}^{2.5}$ ,  $0.025 \mu\text{m} < a < 0.25 \mu\text{m}$ .

The X-ray halo surface brightness profiles shown in Figure 3 depend strongly on the grain diameter used in the single-size grain distributions: smaller grains give rise to more scattering at large angles, and the inner halo surface brightness is reduced. Similarly, the brightness of the inner halo (which is dominated by larger grains) computed using the MRN grain model is comparable to the brightness computed using the  $a = 0.2 \mu\text{m}$  single-size grain distribution, but the smaller grains included in the MRN distribution give rise to slightly more scattering at larger angles.

Finally, we estimate the X-ray halo surface brightness profile expected for a point source located in a distant, dusty galaxy. We specifically consider the case of M87, and thus assume a distance  $D = 14.7 \text{ Mpc}$  (Jacoby, Ciardullo, & Ford 1990) and Galactic latitude  $b = 74^\circ.5$ . In our own Galaxy we adopt the spatial distribution of gas and dust given by MG, where the gas density is constant in planes parallel to the Galactic plane, and decreases exponentially outward with a scale height of 100 pc. For simplicity, we assume the same gas/dust distribution in M87 as well (except we take  $b = 0^\circ$ ). Thus, the density along the line of sight to an object located a distance  $D$  (kpc) at a Galactic latitude  $b$  is

$$\rho(x) = \rho_0 \{ \exp[-10xD(\text{kpc}) \sin b] + \exp[-10(1-x)D(\text{kpc})] \}, \quad (7)$$

so that the function  $f(x)$  in equation (5) is given by

$$f(x) = \frac{\rho(x)}{\int_{x=0}^{x=1} \rho(x) dx}.$$

Shown in Figure 4 is the resultant X-ray halo surface brightness profile versus observation angle using the MRN grain-size model, and as a function of photon energy. The profiles are characterized by a large-diameter outer halo due to scattering by dust in our own Galaxy, and by a much

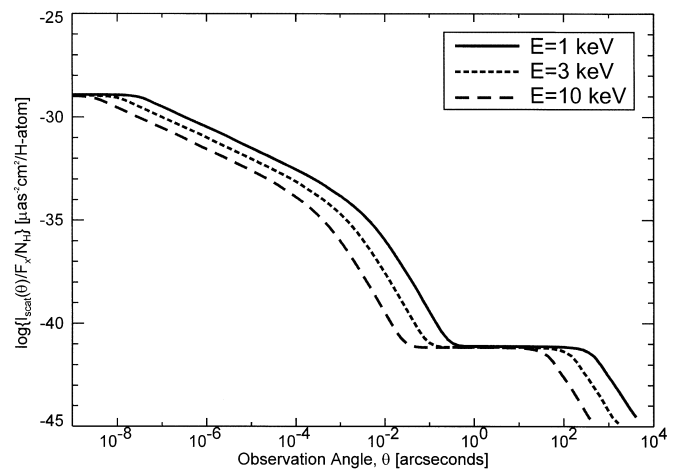


FIG. 4.—Relative X-ray halo surface brightness as a function of observation angle  $\theta$  expected for a point source in M87 ( $D = 14.7 \text{ Mpc}$ ,  $b = 74^\circ.5$ ), assuming the dust/gas distribution function described by MG (eq. [7]), and for the MRN dust grain model.

smaller inner microhalo due to scattering by dust within M87. The surface brightness in the central  $\mu\text{as}^2$  of the inner halo is more than 12 orders of magnitude brighter than that of the outer halo. Note, however, that since it subtends a solid angle that is smaller by a factor of  $\sim 10^{16}$ , it contains only a tiny fraction of the total halo energy. For example, at 1 keV the total intensity of the halo brightness profile (relative to the source flux) integrated over the range  $10^{-9''} < \theta < 0.1''$  is  $3.7 \times 10^{-27} [\text{cm}^2 (\text{H atom})^{-1}]$ , while the profile integrated from  $0.1'' < \theta < 1000''$  is  $6.5 \times 10^{-24} [\text{cm}^2 (\text{H atom})^{-1}]$ . Carter, Johnstone, & Fabian (1997) estimate that the H column in the core of M87 is at least  $10^{18} \text{cm}^{-2}$  or possibly several orders of magnitude greater; nonetheless, even with a  $\mu\text{as}$ -resolution instrument having very high sensitivity, the H column density is probably many orders of magnitude too small to detect the inner microhalo in this case.

#### 4. CONCLUSION

We have found that the scattering of X-rays by interstellar dust clumped very close to the source gives rise to a bright, small-diameter X-ray halo. This prediction, while somewhat surprising, is easy to understand. As Figure 1b shows, if the same amount of material is placed at different values of  $x$ , the intensity rises as  $(1 - x)^{-2}$ . Since  $1 - x$  represents the distance from the scatterer to the source, this inverse square relationship merely represents the larger flux incident per square centimeter of scatterer due to its proximity to the source. The small halo diameter represents the

angular extent of the distant region that subtends arcminutes as viewed from the (much closer) source. Figure 1a shows the intensity variation to be expected when the scatterer is distributed uniformly along the line of sight. In this case the surface brightness rises as  $(1 - x)^{-1}$ , the same behavior as seen in Figure 1b but modified by the uniformity constraint that places a factor of  $(1 - x)$  less material to scatter at any distance.

In spite of its large relative surface brightness, a large amount of dust undoubtedly will be required to observe an inner microhalo. As a corollary, our results suggest that X-ray scattering by interstellar dust grains should not interfere with subarcsecond imaging observations along extremely dusty lines of sight, as toward the Galactic center or toward the center of other dusty galaxies. Furthermore, it might be possible to use a sufficiently sensitive,  $\mu\text{as}$ -resolution X-ray telescope (i.e., an X-ray interferometer) to measure the detailed X-ray halo surface brightness profile surrounding a source and thus determine the spatial distribution of dust grains along the line of sight and close to the source. That is, if the dust grains were contained in a series of clouds distributed along the line of sight to the source, then the resultant X-ray halo profile would exhibit a series of shoulders, where the angular diameter of each shoulder would be determined by the relative position along the line of sight of the corresponding dust cloud.

We would like to thank the referee, Chris Mauche, for many helpful comments and suggestions.

#### REFERENCES

- Bode, M. F., Priedhorsky, W. C., Norwell, G. A., & Evans, A. 1985, *ApJ*, 299, 845  
 Carter, D., Johnstone, R. M., & Fabian, A. C. 1997, *MNRAS*, 285, L20  
 Catura, R. C. 1983, *ApJ*, 275, 645  
 Gallagher, D., Cash, W., & Green, J. 1995, *ApJ*, 439, 976  
 Henke, B. L., Gullikson, E. M., & Davis, J. C. 1993, *At. Data Nucl. Data Tables*, 54  
 Jacoby, G. H., Ciardullo, R., & Ford, H. C. 1990, *ApJ*, 356, 332  
 Mathis, J. S., Cohen, D., Finley, J. P., & Krautter, J. 1995, *ApJ*, 449, 320  
 Mathis, J. S., & Lee, C.-W. 1991, *ApJ*, 376, 490 (ML)  
 Mathis, J. S., Rumpl, W., & Nordsieck, K. H. 1977, *ApJ*, 217, 425 (MRN)  
 Mauche, C. W., & Gorenstein, P. 1986, *ApJ*, 302, 371 (MG)  
 \_\_\_\_\_. 1989, *ApJ*, 336, 243  
 Predehl, P., Bräuninger, H., Burkert, W., & Schmitt, J. H. M. M. 1991, *A&A*, 246, L40  
 Predehl, P., & Klose, S. 1996, *A&A*, 306, 283  
 Predehl, P., & Schmitt, J. H. M. M. 1995, *A&A*, 293, 889  
 Rolf, D. P. 1983, *Nature*, 302, 46  
 Smith, R. K., & Dwek, E. 1998, *ApJ*, 503, 831 (SD)  
 Woo, J. W., Clark, G. W., Day, C. S. R., Nagase, F., & Takeshima, T. 1994, *ApJ*, 436, L5